Magnetotransport of the Sinai billiard

M. Fließer,* G. J. O. Schmidt, and H. Spohn†
Theoretische Physik, Ludwig-Maximilians-Universität, Theresienstrasse 37, 80333 München, Germany
(Received 29 January 1996)

We study numerically the magnetotransport of the two-dimensional Sinai billiard in a uniform magnetic field. We argue that one must include impurity scattering in order to have a well-posed physical problem. Still, there is a window for the scattering time where the transport is dominated by the deterministic dynamics. We investigate the dynamical structure of phase space, peaks in the magnetoresistance and conductance, and diffuse instead of specular reflection. [S1063-651X(96)07906-8]

PACS number(s): 05.45.+b, 05.60.+w

I. INTRODUCTION

The Sinai billiard is presumably the simplest *strictly mechanical* system that has a finite, nonzero Ohmic resistance: One starts with a fundamental domain in the plane, which we take as the unit square $\mathcal{D}=[0,a]\times[0,a]$. Inside $\mathcal{D}$ we place (a few) stictly convex and nonoverlapping scatterers. This arrangement is repeated periodically over the full plane. A mechanical point particle starts in the region outside the scatterers. The particle moves according to its velocity along a straight line until it hits a scatterer, where it is elastically reflected; i.e., at a collision the angle of incidence and of reflection are equal. This dynamic is continued *ad infinitum*. It is proved [1,2] (with one proviso, which will be explained below) that due to the many collisions the trajectory resembles (in a statistical sense) a random walk. Typically the position of the particle, $\mathbf{x}(t)$, will grow proportional to $\sqrt{t}$ for large t.

What may look like a theoretical toy model has in fact been realized to a good approximation experimentally in the form of a lattice of antidots [3–5]. This is a two-dimensional electron film at a semiconductor interface on which geometrical restrictions of the form described before are imposed, e.g., by lithographically structured electrodes. Within good accuracy the dynamics of the electrons is strictly two dimensional, independent, and classical, since the lattice constant ($a\approx 200-500$ nm) is much larger than the Fermi wavelength (≈ 50 nm). Experimentally one measures the magnetotransport, i.e., the magnetoresistance and Hall resistance, in dependence on the magnetic field, which can be easily varied.

The dynamical problem thus posed is the Sinai billiard in a uniform external magnetic field B, perpendicular to the plane. In fact, geometrically this is a very natural modification. Rather than along a straight line, between two collisions the particle moves now on a circle with radius $r_c=m^*v/eB$ and tangent to its velocity, where m^* denotes the effective mass, e the charge, and v the speed of the particle. Experimentally values down to $r_c/a\ll 1$ can be reached.

We will take the antidot lattice as our guideline. However, the true electrostatic antidot potential is not exactly a Sinai scatterer and one should worry also about other imperfections. Our goal here is *not* to optimize the classical description of a particular antidot probe. Rather we would like to understand, within the framework of a simplified but definite model system, how properties of the deterministic dynamics are reflected in the magnetotransport.

In the Sinai billiard, even including other scattering mechanisms to be explained below, there is no energy dissipation. Therefore an external electric field would eventually accelerate the particle and no steady current could be established. This heating is only second order in the electric field, but it forces us to define transport through linear response. The Ohmic conductivity is then proportional to the diffusivity via an Einstein relation.

At this stage it may be useful to view the diffusive growth of the position $\mathbf{x}(t)$ in a slightly different way, still restricting ourselves to the case $B=0$. We consider the dynamics on $\mathcal{D}$ with periodic boundary conditions, i.e., on the unit torus T^2 (setting the lattice constant $a=1$). The velocity of the particle is denoted by $\mathbf{v}(t)$. By conservation of energy we may normalize as $|\mathbf{v}(t)|=1$ and set $\mathbf{v}=(\cos\phi,\sin\phi)$. Let $\Lambda\subset T^2$ be the allowed position space with area $|\Lambda|$. The phase space of the billiard is then $\Gamma=\Lambda\times S^1$. It comes with the *invariant microcanonical measure* $d\mu=|\Lambda|^{-1}dx_1dx_2d\phi/2\pi$. With respect to μ, $\mathbf{v}(t)$ is a stationary stochastic process. $\mathbf{v}(t)$ is mixing and, in fact, enjoys the much stronger ergodic property of positive Kolmogorov-Sinai entropy [6]. Clearly, the position of the particle in the plane is given by

$$\mathbf{x}(t)=\mathbf{x}(0)+\int_0^t ds\mathbf{v}(s). \tag{1}$$

Diffusion for $\mathbf{x}(t)$ results from the chaotic dynamics of $\mathbf{v}(t)$ on Γ. More specifically

$$\frac{1}{\sqrt{t}}\int_0^t ds\mathbf{v}(s) \tag{2}$$

must satisfy the central limit theorem [note that $\langle\mathbf{v}(t)\rangle=0$, average with respect to μ]. Its covariance is the diffusion tensor

*Electronic address: fliesser@stat.physik.uni-muenchen.de
†Electronic address: spohn@stat.physik.uni-muenchen.de

$$D_{\alpha\beta}=\frac{1}{2}\int_{-\infty}^{\infty}dt\langle v_\alpha(t)v_\beta(0)\rangle, \tag{3}$$

$\alpha,\beta=1,2$. D is symmetric, but nondiagonal in general, the diagonal being related to the mean square displacement as $\langle x_\alpha(t)^2\rangle\cong 2D_{\alpha\alpha}t$ for large t.

In parentheses we remark that the central limit theorem does *not* follow abstractly from a positive Kolmogorov-Sinai entropy. For example, as can be seen from (3), a sufficiently fast decay of $\langle v_\alpha(t)v_\beta(0)\rangle$ is needed. The proof of the central limit theorem requires a uniformly bounded time between collisions [2]. This is the condition of finite horizon because no unbroken trajectory reaches infinity. In that case and for standard geometries such as a triangular lattice $\langle v_\alpha(t)v_\beta(0)\rangle$ seems to decay exponentially (with oscillations) [7] and $\langle x_\alpha(t)^2\rangle$ reaches its linear asymptotics after a few (5–10) collisions.

In the following we will consider the particular case of a single circular scatterer per unit cell with radius R, $0<R<a/2$. Clearly, the time between collisions is unbounded. $\langle v_\alpha(t)v_\beta(0)\rangle$ decays as $1/t$, $\langle x_\alpha(t)^2\rangle$ grows as $t\ln t$, and strictly speaking $D_{\alpha\alpha}=\infty$ [8,9]. This infinity is the result of an overidealization. In real systems scattering by impurities may be rare, but is unavoidable. The most perfect antidot samples have an impurity mean free path of the order of 10^5 nm. In the Sinai billiard impurity scattering is introduced simply by randomizing, at the current position, the velocity angle ϕ at Poisson distributed random times with mean spacing τ. $\mathbf{v}(t)$ is then no longer deterministic, but (3) remains valid provided $\langle\rangle$ is understood as double average, i.e., with respect to the initial conditions and the impurity scattering at random times. The diffusion matrix depends now on τ. Clearly, if $\tau\to 0$ any trace of the deterministic dynamics is washed out and $D_{\alpha\beta}(\tau)\cong\langle v^2\rangle\tau\delta_{\alpha\beta}$. On the other hand, for the square lattice, $D(\tau)\to\infty$ as $\tau\to\infty$. We argue here that there is a meaningful τ window (*which has to be determined*), where D is dominated by the deterministic dynamics, yet the long collisionless trajectories are suppressed by impurity scattering.

After these preliminaries we turn to the problem of interest, namely, $B\neq 0$. Antidot probes are maintained at Kelvin temperatures. Therefore the electrons have a velocity distribution uniform over the disk $\{\mathbf{v}||\mathbf{v}|\leq v_F\}$ with v_F the Fermi velocity. Following standard linear response the magnetoconductance is obtained as

$$\sigma_{\alpha\beta}=\frac{e^2m^*}{\pi\hbar^2}v_F^2\int_0^{\infty}dt\langle v_\alpha(t)v_\beta(0)\rangle. \tag{4}$$

Here $-e$ is the charge, m^* the effective mass of the electron, and, as before, $\langle\ \rangle$ the microcanonical average with $|\mathbf{v}|=1$. By stationarity $\langle v_\alpha(t)v_\beta(0)\rangle=\langle v_\beta(-t)v_\alpha(0)\rangle$. Thus

$$D_{\alpha\beta}=\frac{\pi\hbar^2}{e^2m^*v_F^2}\frac{1}{2}(\sigma_{\alpha\beta}+\sigma_{\beta\alpha}). \tag{5}$$

In particular, the diagonal matrix elements $\sigma_{\alpha\alpha}$ are determined by the mean square displacement of the diffusing particle. Unfortunately, the off-diagonal elements of σ cannot be related to diffusion in a position which complicates a qualitative understanding of their parameter dependence. For $B=0$ invariance under time reversal implies $\langle v_\beta(-t)v_\alpha(0)\rangle=\langle v_\beta(t)v_\alpha(0)\rangle$ and thus $\sigma_{\alpha\beta}=(e^2m^*/\pi\hbar^2)D_{\alpha\beta}$, which is the Einstein relation for a classical gas with $T=0$ Fermi velocity distribution. In the case of a square lattice, considered here, one has the additional reflection symmetry $x_1\mapsto\pm x_1, x_2\mapsto\mp x_2, B\mapsto -B$. Together with time reversal $t\mapsto -t, B\mapsto -B$, this implies $\langle v_\alpha(t)v_\beta(0)\rangle=(-1)^{\alpha+\beta}\langle v_\alpha(-t)v_\beta(0)\rangle$ for arbitrary B. Therefore $D_{11}=D_{22}$, $D_{12}=0$, and $\sigma_{12}=-\sigma_{21}$.

The resistance matrix ρ is the inverse of σ, explicitly given by

$$\rho_{11}=\frac{\sigma_{11}}{\sigma_{11}\sigma_{22}+\sigma_{12}\sigma_{21}},\quad \rho_{12}=\frac{\sigma_{12}}{\sigma_{11}\sigma_{22}+\sigma_{12}\sigma_{21}} \tag{6}$$

and correspondingly for ρ_{22},ρ_{21}. Usually ρ_{11} is called the magnetoresistance and ρ_{12} the Hall resistance.

For very small B the trajectories between collisions are almost straight and one may use perturbation techniques developed in [10] with the result that the properties at $B=0$ persist. On the other hand, as $B\to\infty$, the trajectories are either closed circles or skip along a single scatterer (rosette orbits). The dynamics is then integrable. Thus for intermediate values we expect a mixed phase space. Its structure will be discussed in detail in Sec. II. We only remark that for the square lattice we will find orbits drifting to infinity. But in contrast to the case $B=0$, for a certain B range these orbits form a set of positive measure. (4) is then ill defined. Also restricting $\langle\rangle$ to some part of the phase space is rather *ad hoc*. As argued above and *a forteriori* for $B\neq 0$, the correct physical setting is to introduce scattering by impurities. The derivation of (4) remains valid and yields a well-defined σ depending on τ. As $\tau\to 0$ the conductance is completely determined by impurity scattering. The problem of interest and to be studied in Sec. III is the behavior of $\sigma(\tau)$ for reasonably large values of τ. In particular we will have to find out which piece of the deterministic dynamics dominates $\sigma(\tau)$.

In our paper we study only the square lattice with disk scatterers (antidots). The parameters are then (1) the external magnetic field B, equivalently the gyration radius r_c/a, (2) the antidot radius R/a, (3) the impurity scattering mean free path $l/a=|\mathbf{v}|\tau/a$, equivalently the mean free time τ, $\tau=l$ for $|\mathbf{v}|=1$. All three parameters are measured in units of the lattice spacing a, which we set equal to 1. Typical experimental values are $R/a\approx 1/6$, $r_c/a\approx 2$, and $l/a\approx 10$. The transport coefficients of interest are the magnetoconductance and Hall conductance σ_{11},σ_{12} as given by (4) and the corresponding resistances of (6).

Antidots have some intrinsic roughness from the lithographic preparation process. We can model this through diffuse scattering: when the particle hits an antidot it is specularly reflected with probability p and diffusely with probability $1-p$, $0\leq p\leq 1$. This means that relative to the normal the outgoing angle θ is chosen at random according to the distribution $\cos\theta d\theta/2, -\pi/2\leq\theta\leq\pi/2$, which just ensures that the microcanonical measure μ is left invariant. The influence of diffuse scattering on the transport properties will be discussed in Sec. V.

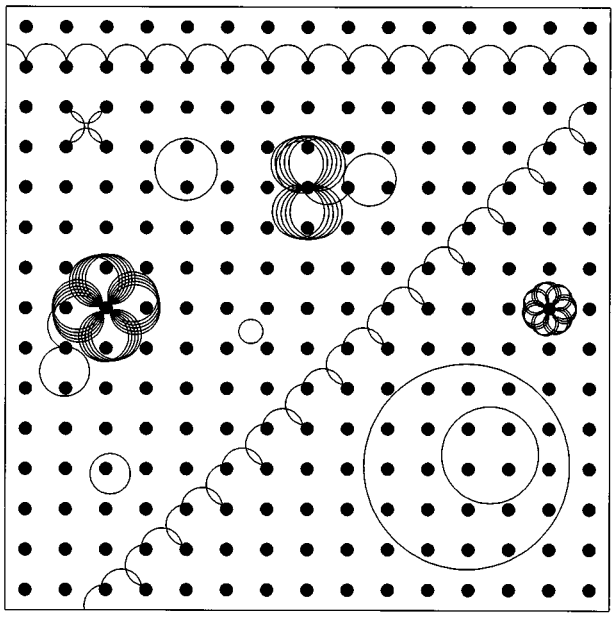

FIG. 1. Various orbits for $R=0.15$

II. DYNAMIC STRUCTURE OF THE PHASE SPACE

In this section we study the deterministic dynamics setting $\tau=\infty$. By definition the phase space Γ refers to a single unit cell. Its various components are, however, more easily characterized in the periodically repeated scheme of Fig. 1. For $r_c<\frac{1}{2}-R$ the billiard is completely integrable. Orbits are either circles around zero, circles around a single scatterer, or rosettes skipping along a single scatterer; cf. Fig. 1. For r_c sufficiently large the billiard is fully chaotic. For intermediate values of r_c the chaotic sea Γ_c coexists with a regular piece $\Gamma_0=\Gamma\setminus\Gamma_c$, for which by definition the Lyapunov exponent vanishes. Γ_c seems to consist of one single component with the exception of a set of tiny measure. Figure 2 gives the ''phase'' diagram in parameter space, indicating where the system is integrable, mixed, and fully chaotic.

Γ_0 splits into several dynamically distinct components. First of all, there are collision-free circular orbits; cf. Fig. 1. They encircle either zero, one, or several scatterers. Therefore the latter are also called pinned orbits. In Fig. 2 we plot

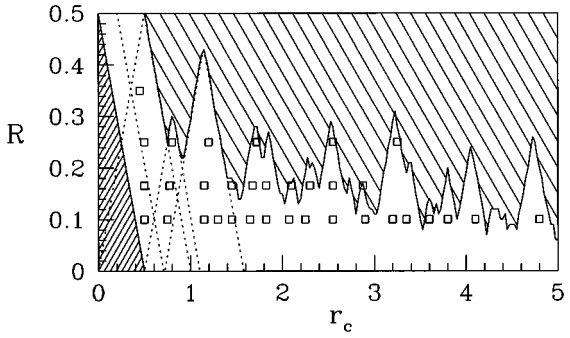

FIG. 2. Phase diagram in parameter space. (///) is completely integrable, (\\\) is fully chaotic, and the remainder mixed dynamics. $(\cdots)$ are the boundaries of the 0-, 1-, 2-, and 4-circles. □ denotes the location of peaks in ρ_{11} for various values of R; compare Fig. 8.

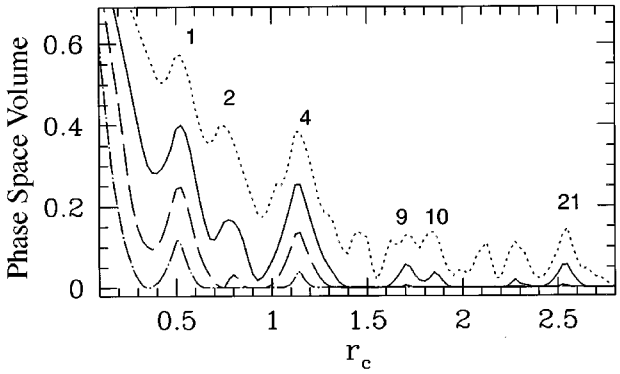

FIG. 3. Phase space volume of all circle orbits for $R=0.1$, 0.167, 0.25, and 0.35 from top to bottom.

the first few boundaries in parameter space, which limit regions where 0-circles cease to exist, 1-circles start and cease to exist, etc. These boundaries are determined by purely geometric conditions. For large r_c they form a fairly complicated pattern, which is responsible for the rugged boundary between the mixed and fully chaotic ''phase,'' where we simply assume that the absence of circle orbits is equivalent to fully chaotic dynamics. This is not evident and there could be other regular orbits. However, if they exist at all, they must have minute phase space volume.

A dynamically important information is the phase space volume of all circle orbits, which is displayed in Fig. 3. Clearly the 0-, 1-, 2-, and 4-circles dominate (for suitable R), but also orbits encircling 3, 7, 9, 10, 14, 16, 21, ... scatterers have a distinguishable weight.

Circular orbits are marginally stable. There is a further set of marginally stable orbits, namely, the rosette orbits; cf. Fig. 1. Their angle of incidence does not change under successive collisions. Thus a typical rosette orbit is quasiperiodic and not closed. Because of this precession there cannot be a set of positive measure of rosette orbits that encircle other scatterers. Rosette orbits cease to exist for $r_c>0.5$. However, for small r_c rosette orbits make up a substantial part of Γ_0. We note that in phase space the boundaries of rosette and circle components are piecewise smooth, because they are determined geometrically.

Figure 4 is a Poincaré plot, where we map from outgoing to outgoing collision. We use the angle on the surface of the scatterer, $s\in[0,2\pi]$, and the angle of the velocity relative to the normal θ, $|\theta|\leq\pi/2$, as coordinates. For $r_c=0.4$ we rec-

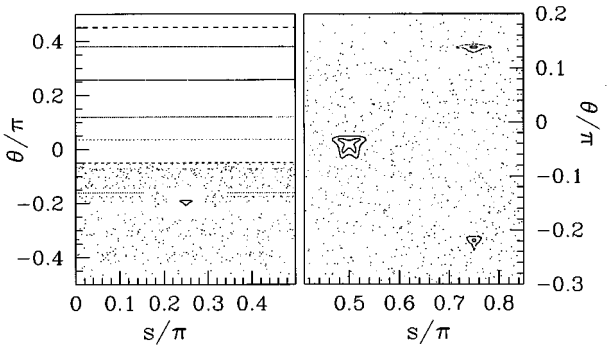

FIG. 4. Poincaré sections for $r_c=0.4$, $R=0.15$ (left) and $r_c=0.51$, $R=0.25$ (right).

ognize the rosette orbits with $\theta \geqslant -0.05\pi$. Rosettelike segments of chaotic trajectories appear as lines with constant θ in the chaotic sea, whereas the circle orbits are hidden for our choice of section. Also several elliptic islands of the familiar structure are clearly visible. These are hard to classify systematically and we proceed via case study. An obvious example is Fig. 1 (top) [11], which corresponds to a fixed point of the return map. From a linear stability analysis, this fixed point is stable provided

$$\left| 1 - \frac{2\,r_c}{R} \cos \arcsin\left(\frac{1}{2\,r_c} \right) \right| \leqslant 1. \tag{7}$$

For example, for $R=0.25$ the fixed point is stable for $0.5<r_c<0.56$. At the lower end the fixed point becomes marginally stable and the elliptic island disappears. At the upper end there is a pitchfork bifurcation to a stable period-2 orbit, which corresponds to a sequence of a long, a short, a long, etc. ''jumps'' from scatterer to scatterer. At $r_c=0.57$ the period-2 orbit becomes unstable and the island ceases to exist. The phase space volume correponding to the island is small, reaching a maximum of 0.008 in the interval $0.505 \leqslant r_c \leqslant 0.525$.

The orbits shown in Fig. 1 (top) drift with a constant velocity to infinity. For this reason we call them ''drifting orbits.'' Encouraged by our example we look for other drifting orbits constructed according to the same rule. We label such fixed points by their Miller index, (1,0) in our example. There is a (3,0) island existing only for $R<0.11$ with even smaller phase space volume than the (1,0) island. It should be noted that the linear stability is only a necessary condition. Given a stable fixed point, the orbit may interfere with the row of scatterers in parallel and thus in fact not exist at all, as for the (1,1) or the (2,0) island. A further example is Fig. 1 (diagonal). This a stable period-2 orbit of the Poincaré map, which alternates between (1,0) and (0,1). For $r_c=0.51$ (which is favored by the stability condition) we determined numerically the measure of all drifting orbits. They come into existence at $R=0.1$, reach their maximal phase space fraction of 0.015 at $R \cong 0.3$, and then disappear at $R \cong 0.38$. We conclude that drifting orbits are dynamically distinct. However, they exist only in a fairly small window and even then have only small measure. Still, if we would stick to the fully deterministic dynamics, according to (4) they would eventually dominate the magnetotransport.

In the Poincaré section, one also finds elliptic islands that do not correspond to drifting orbits. An example is the closed orbit in Fig. 1 (top left), a period-4 fixed point of the return map from the small island in Fig. 4 for $r_c=0.4$. Also at $r_c=0.6$, $R=0.25$ there is a stable periodic orbit that skips along nine scatterers before returning to its original phase. Each of these regular islands exists only for a small parameter range and again their phase space volume is minute.

For the billiard at $B=0$ the trajectories drifting straight to infinity form a set of measure zero. Still chaotic trajectories follow an exceptional trajectory for a long time leading to the nonintegrable decay of $\langle v_\alpha(t) v_\beta(0) \rangle$. For lack of a better name we call such orbits ''sticky.'' A sticky orbit belongs to the chaotic phase space but follows a nearby regular orbit for a long time. Once a sticky orbit escapes the regular neighborhood it is unlikely to return. A regular piece of phase space has a sticky boundary if chaotic orbits close to the boundary stick around for a long time. For $B \neq 0$ we also expect sticky orbits. Of course, at this stage it is not clear whether this phenomenon will be of any importance to the magnetotransport.

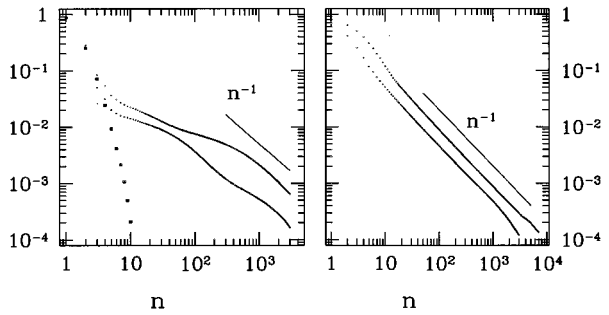

FIG. 5. (a) Probability of n successive (1,0) jumps for a chaotic trajectory, $R=0.25$ (upper curve), $R=0.28$ (middle curve), and $R=0.36$ (lowest dots), $r_c=0.51$. (b) probability of colliding n times with the same scatterer for a chaotic trajectory, $R=0.1$ (lower curve) and $R=0.05$ (upper curve), $r_c=0.65$.

For drifting orbits we expect a scenario that is well understood for smooth potentials [12–14]. An elliptic island is surrounded by a self-similar hierarchy of cantori. The motion can be modeled as a Markov process jumping from level to level in that hierarchy. The waiting time increases exponentially with the level, which leads then to slow motion and a power law decay of correlations. When applying this scenario to one island of drifting orbits, one has to recall that the self-similar structure may be cut off at a certain level by geometric constraints. We investigate the (1,0) drifting orbits at $r_c=0.51$. We determine the probability of the sticky chaotic trajectories that follow the drifting orbits over n collisions, i.e., for the (1,0) island ''jump'' n times by the lattice vector (1,0). For $R=0.25$ and 0.257 we seem to get an algebraic decay approximately as $1/n$ for long times. On the other hand, for $R=0.33$ we have a quick drop and a logarithmic plot confirms exponential decay. We interpret this behavior as coming from a geometric constraint.

Circular and rosette orbits are not surrounded by chains of islands and cantori, because they are geometrically constrained by a scatterer. Periodic rosette orbits encircling other scatterers form a set of measure zero. Yet sticky chaotic trajectories can follow the rosette over many collisions (cf. Fig. 1) if we choose their angle of incidence just below that of the rosette. If n collisions are followed, the phase space volume scales as $1/n$. To test this prediction we measured the probability that an orbit collides n times with the same scatterer. Figure 5 confirms well our picture. For circle orbits this effect has smaller phase space volume and we expect a faster decay proportional to $1/n^2$. Circle orbits seem to be ''less sticky'' than rosettes.

The degree of mixing of the chaotic component Γ_c of phase space is quantitatively characterized by the Lyapunov exponent, which we plot in Fig. 6 for the continuous time dynamics. In the fully chaotic ''phase'' we see a weak, monotonic increase. If a regular component is coexisting, we have pronounced oscillations. Somewhat to our surprise the maxima are well correlated to the occurrence of circle orbits.

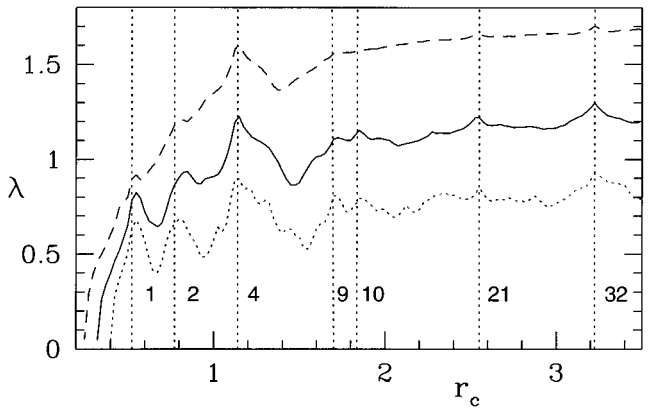

FIG. 6. Lyapunov exponent for $R=0.1$ $(\cdots)$, 0.167 (–), and 0.25 $(--)$. Vertical lines indicate the location of maximal phase space volume of circle orbits labeled the number of encircled scatterers.

III. IMPURITY SCATTERING

As argued in the Introduction, the physically meaningful definition of the magnetotransport is given by

$$\sigma_{\alpha\beta}=\int_0^\infty dt C^\tau_{\alpha\beta}(t). \tag{8}$$

To simplify we normalized here the prefactor to one and, for the purpose of this section only, we indicate explicitly the τ dependence. $C^\tau_{\alpha\beta}(t)=\langle v_\alpha(t)v_\beta(0)\rangle$ is the (stationary) velocity autocorrelation including impurity scattering with mean free time τ. The deterministic correlation is denoted by $C_{\alpha\beta}(t)=\lim_{\tau\to\infty}C^\tau_{\alpha\beta}(t)$. In antidot probes τ ranges from 5 to 100 in our units.

If at each impurity scattering we would not only randomize the velocity but also the position over the current unit cell, then the so obtained velocity autocorrelation equals $e^{-t/\tau}C_{\alpha\beta}(t)$ because $\langle\mathbf{v}\rangle=0$ immediately after the first impurity scattering. For the more physical impurity scattering adopted here we still expect

$$C^\tau_{\alpha\beta}(t)\cong e^{-t/\tau}C_{\alpha\beta}(t) \tag{9}$$

to be a reasonable approximation over the parameter range of interest [15,16], however, still conditional to a numerical check. As explained in Sec. II the phase space decomposes as $\Gamma_c\cup\Gamma_d\cup\Gamma_r$, Γ_d the drifting orbits, Γ_r the circle, rosette, and nondrifting regular orbits, with probability μ_c,μ_d,μ_r, respectively (some of which could vanish). Then obviously

$$C_{\alpha\beta}(t)=\mu_c C^{(c)}_{\alpha\beta}(t)+\mu_d C^{(d)}_{\alpha\beta}(t)+\mu_r C^{(r)}_{\alpha\beta}(t), \tag{10}$$

where $C^{(z)}_{\alpha\beta}(t)$ is the deterministic velocity autocorrelation over the normalized z component of Γ. We combine now (10) and the approximation (9) to discuss $\sigma(\tau)$.

If τ is sufficiently large, so that $e^{-t/\tau}$ decays more slowly than $C^{(c)}_{\alpha\beta}(t)$, then

$$\int_0^\infty dt e^{-t/\tau}C^{(c)}_{\alpha\beta}(t)\cong\int_0^\infty dt C^{(c)}_{\alpha\beta}(t)\equiv S_{\alpha\beta}. \tag{11}$$

In fact the $\cong$ is a little bit delicate. Presumably, because of sticky orbits, $C^{(c)}_{\alpha\beta}(t)$ has a slow decay, similarly as in the known case $B=0$. Our numerical procedure causes an effective numerical cutoff in t and we do not see contributions from such a slow decay. Thus we expect that over the range $5\leqslant\tau\leqslant\tau_{\max}$ (11) is essentially τ independent and determined by the chaotic dynamics. For $\tau>\tau_{\max}$ the slow decay would become significant. $\tau_{\max}$ seems to be so large that it cannot be accessed by our numerics. Note that for large r_c there are no collisionless trajectories running to infinity which guarantees a finite horizon and a well-defined transport even without impurity scattering.

For the drifting orbits $C^{(d)}_{\alpha\alpha}(t)=(\langle v_\alpha\rangle_d)^2$ as $t\to\infty$, where $\langle v_\alpha\rangle_d$ is the average drift velocity along the α axis. Together with (9) this yields the contribution

$$\mu_d(\langle v_\alpha\rangle_d)^2\tau \tag{12}$$

to $\sigma(\tau)$. μ_d is always small. Even if we adjust μ_d to its maximum we still have to make $\tau\geqslant100$ in order to obtain a significant contribution. Therefore in the following we neglect the contribution (12). Still, provided $\mu_d\neq0$, as τ is increased, $\sigma(\tau)$ will be dominated by (12) rather than by a possibly slow decay in (11).

The dominant contribution to the third piece $C^{(r)}_{\alpha\beta}(t)$ is from circle orbits, oscillating with the cyclotron frequency $\omega_c=1/r_c$. Thus

$$\int_0^\infty dt e^{-t/\tau}C^{(r)}_{\alpha\beta}(t)\cong\sigma^D_{\alpha\beta}, \tag{13}$$

which by definition is the Drude magnetoconductance

$$\sigma^D_{11}=\frac{\tau}{1+(\omega_c\tau)^2},\quad \sigma^D_{12}=\frac{\omega_c\tau^2}{1+(\omega_c\tau)^2}. \tag{14}$$

For the diagonal matrix elements $\sigma^D_{11}\ll S_{11}$ and thus

$$\sigma_{11}\cong\mu_c S_{11} \tag{15}$$

while for the Hall conductance we obtain

$$\sigma_{12}\cong\mu_c S_{12}+(1-\mu_c)\sigma^D_{12}. \tag{16}$$

Figure 7 shows a comparison between numerically determined values of $\sigma_{\alpha\beta}(\tau)$ for two different values for τ and the approximations (15), (16). The accordance is indeed very good, even for fairly small values of τ. We conclude that magnetotransport is dominated by the chaotic dynamics over the whole physically accessible range $5\leqslant\tau\leqslant100$. In the following section we set $\tau=10$ with the understanding that except for finer details we observe indeed the deterministic dynamics as given through (15), (16).

IV. MAGNETOTRANSPORT

In Fig. 8 we show the magnetoresistance ρ_{11}, as determined by (6) and (8) with $\tau=10$, as a function of r_c for various values of R. Such pronounced peaks have also been observed experimentally [4,17–19] and in numerical simulations with a smooth scatterer potential [15,16].

A first guess might be that ρ_{11} reflects the variation in the

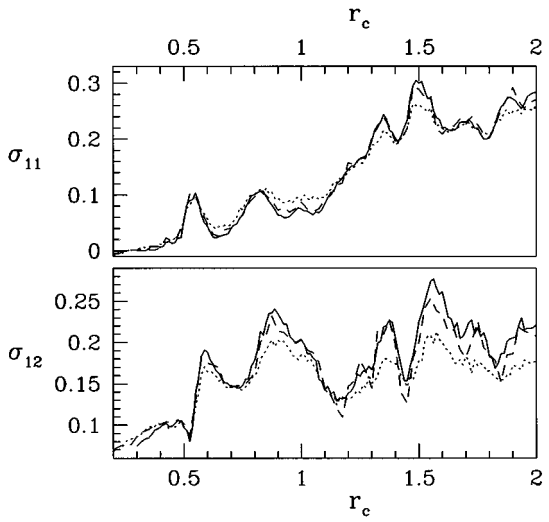

FIG. 7. Conductance under the full dynamics including impurity scattering with $\tau=40$ $(--)$, $\tau=10$ $(\cdots)$, and in the approximation of Eqs. (15) and (16) (—), $R=0.167$.

chaotic phase space volume μ_c. However, using (15), (16) together with the numerically determined μ_c from Fig. 3 we find that the resulting variation in ρ_{11} is a factor 4–10, in some cases even 100, too small. Thus we must observe changes $S_{\alpha\beta}$, which is the integrated velocity autocorrelation of the chaotic phase space; cf. (11).

To systematize we indicate the location of the peaks in ρ_{11} by boxes in Fig. 2. They fill all of the mixed phase. In the integrable phase one has Drude behavior, in the chaotic phase the conductances approach their values for $B=0$; i.e., σ_{11} increases and σ_{12} decreases with r_c. The location of the peaks in ρ_{11} changes very little with R. Each column of peaks occurs at those r_c where the orbits encircling a certain fixed number of antidots have maximal phase space volume. Peaks can be labeled with a definite n circle. This works even when the associated phase space volume is very small, such as, e.g., the 7-circle peak.

In view of (6) we would expect that a peak in ρ_{11} is correlated with either a maximum in σ_{11} (see Fig. 9) or a minimum in σ_{12}, or both. To test which we show in Fig. 10 an enlargement for $R=0.16$. σ_{12} has indeed a minimum at $n=1$-, 2-, and 4- peaks. σ_{11} has a maximum at the 1-peak, but the maximum at the 2-peak is somewhat shifted. This

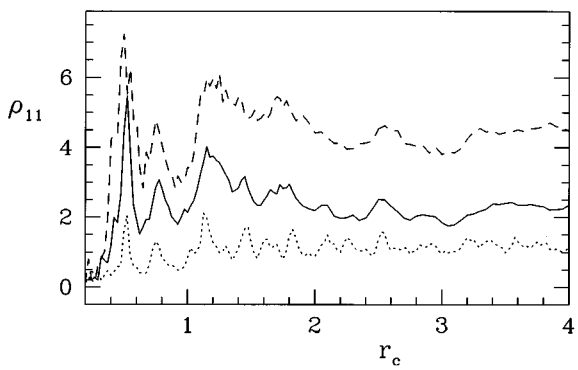

FIG. 8. Magnetoresistance for $R=0.1$ $(\cdots)$, 0.167 (—), and $0.25(--)$.

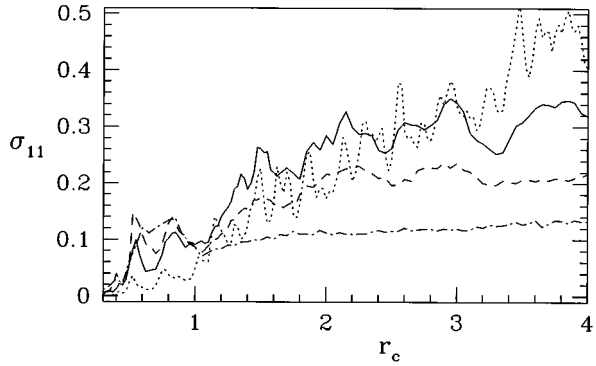

FIG. 9. Magnetoconductance for $R=0.1$ $(\cdots)$, 0.167 (—), 0.25 $(--)$, and 0.35 $(-\cdot-\cdot)$.

small shift in the extremum is actually a fairly frequent property for both σ_{11} and σ_{12}. At the 4-peak σ_{11} has a structureless increase. For the data we analyzed this is an exception. We conclude that at least roughly there is the expected correlation, although the minima in σ_{12} and the maxima in σ_{11} are much less pronounced than the peaks in ρ_{11}.

It has been argued [15] that the peaks in ρ_{11} are due to sticky chaotic trajectories following circle orbits. This would, however, result in a minimum, rather than a maximum, of σ_{11} and such an explanation is not applicable to our model. Sticky behavior of chaotic trajectories is not distinctly correlated with circle orbits, but it is also affected by rosettes, cf. Sec. II. Since the structure in ρ_{11} is so well linked with the occurrence of n-circle orbits, we tried to make a more quantitative connection with $S_{\alpha\beta}$. The various tests were not conclusive and, in our opinion, it is not justified to make a particular class of dynamical trajectories responsible for the peaks in ρ_{11}.

V. DIFFUSE SCATTERING AT EDGES

The edges of real antidots are not completely smooth. The microscopic roughness causes trajectories to be scattered diffusely rather than specularly. In quantum wires, significant modifications of the magnetoresistance are known to be caused by the single parameter p assuming that the trajectory gets scattered diffusely with probability p upon hitting the scatterer. The distribution of the angle of reflection θ relative

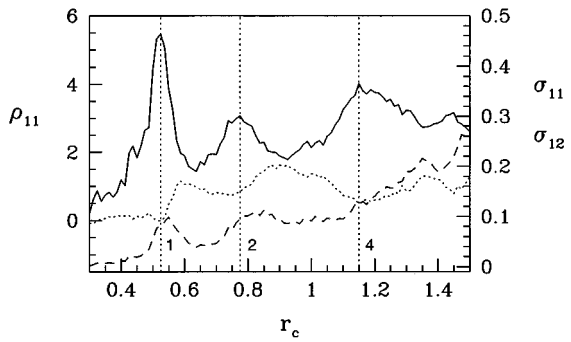

FIG. 10. Magnetoresistance ρ_{11} (—) and magnetoconductance σ_{11} $(--)$, σ_{12} $(\cdots)$ for $R=0.167$.

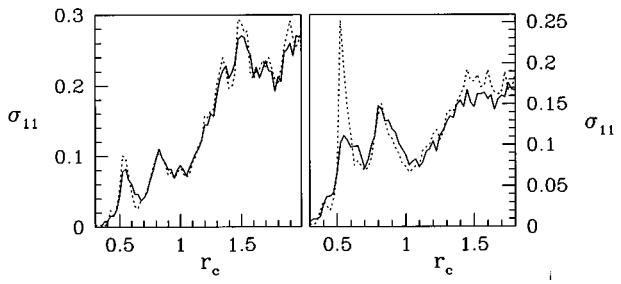

FIG. 11. Conductance with (—) and without ($\cdots$) diffuse scattering for $p=0.5$, $R=0.167$ (left) and $R=0.25$ (right), $\tau=40$.

to the normal equals $\cos\theta d\theta/2$, $|\theta|\leqslant\pi/2$, as required by the invariance under the deterministic dynamics. Experimentally p varies between 0.05 and 0.5 depending on the technique used for creating the potential wells. Here we will use the diffuse scattering mechanism to examine the dynamical origin of some of the peaks in $\sigma_{\alpha\alpha}$ and $\rho_{\alpha\alpha}$ [21].

Circle orbits do not hit a scatterer and are therefore not affected by diffuse scattering. Sticky chaotic trajectories following either drifting orbits or circle and rosette orbits are interrupted by diffuse scattering. The change in transport is, however, quite different in both cases: The contribution of drifting segments to the conductance is proportional to their length. Since the window in the angle θ ensuring a drifting orbit is generally very small, the length of drifting segments in chaotic orbits will be reduced upon diffuse reflection. As a consequence strong diffuse scattering will suppress those features in $\sigma_{\alpha\alpha}$ and $\rho_{\alpha\alpha}$ that are due to drifting orbits. On the other hand for trajectories following circle and rosette orbits not the length of the segments but only the total fraction of such trajectories, e.g., the return probability to a scatterer after one collision, is important. This is not changed by diffuse scattering and thus the features due to circle and rosette orbits will hardly be affected.

To distinguish diffuse scattering from impurity scattering we have to choose a mean free time τ much larger than the average time between collisions with scatterers. Figure 11 compares σ_{11} for the dynamics including diffuse reflection with impurity scattering. The curves are very similar and most peaks remain nearly unchanged. Diffuse scattering essentially corresponds to a reduction in τ. Only the peak at $r_c=0.55$ for $R=0.25$, where we had found the largest island of drifting orbits, is strongly suppressed.

In Fig. 12 we plot ρ_{11} for both cases. The magnetoresistance modulations remain nearly unaffected by the diffuse scattering, and are only smoothed out insignificantly. We can conclude that drifting orbits are of no importance for the peak structure in ρ_{11}.

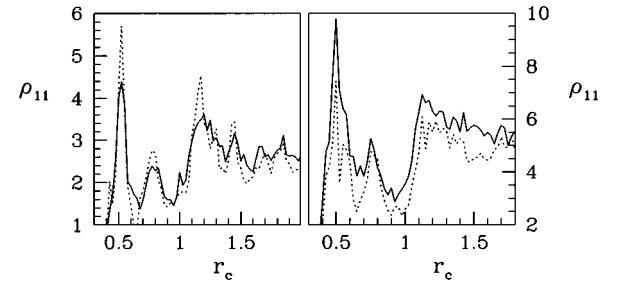

FIG. 12. Resistance with (—) and without ($\cdots$) diffuse scattering for $p=0.5$, $R=0.167$ (left) and $R=0.25$ (right), $\tau=40$.

VI. CONCLUSIONS

We investigated the two-dimensional Sinai billiard with circular scatterers (antidots) on a square lattice and with a uniform external magnetic field. Our numerical studies are considerably more extensive and more systematic than previous work. Of course, we exploit here that the deterministic dynamics is computationally fast. Magnetotransport is studied strictly within linear response theory. There is *no* external electric field acting on the particle. For example, orbits encircling either zero (unpinned) or one scatterer (pinned) make exactly the same contribution to the magnetotransport, because they appear on the same footing in the velocity autocorrelation. Physically, magnetotransport is a well-posed problem only if one includes impurity scattering (with mean free time τ).

Already the very first papers on the subject tried to explain the peaks in the magnetoresistance through chaos in the classical dynamics. This hypothesis has never been tested quantitatively before. Here we demonstrate that there is a reasonably wide τ window, where on one side the chaotic component of the deterministic dynamics dominates [cf. Eqs. (15), (16) together with Fig. 7], and on the other hand drifting and sticky orbits are suppressed. We also include diffuse scattering from antidots, which allows one to access the contribution of drifting orbits to the magnetotransport.

We confirm the pronounced peaks in the resistance as linked to pinned circle orbits. In fact the peaks cover that part of parameter space where the classical dynamics has a mixed phase space. On the other hand, it does not seem to be possible to make one definite class of trajectories responsible for the resistance peaks. We exclude, however, that the drifting and circle orbits make any significant contribution to the magnetotransport. Of course, this does not exclude possible indirect contributions through nearby sticky orbits.

APPENDIX: NUMERICS

Numerically we solve the deterministic dynamics by mapping from collision to collision. Due to the exponential separation of close trajectories according to the Lyapunov exponent (cf. Fig. 6), trajectories can be followed only for 10–20 collisions, limited by the error of initial conditions in double precision. For details of the numerical determination of Lyapunov exponents we refer to [22]. Conductances are calculated by time integrating the velocity autocorrelation $\langle v_\alpha(t)v_\beta(0)\rangle$, diagonal conductances additionally by a linear fit of the mean square displacement $\langle x_\alpha(t)^2\rangle$. Correlations over the chaotic phase space Γ_c are obtained from an average over 10^5 independent segments of one long ergodic trajectory. Velocity autocorrelations typically decay with oscillations within a few (5–10) mean collision times, giving an almost perfect linear growth of the mean square displacement. However, for small $R\leqslant 0.1$ and $r_c\leqslant 1$, in the case of substantial rosette contributions, a slower algebraic decay is visible, requiring segments of length up to 50 collisions. Nu-

merical errors for the integration are about 1–2 %, maximal 5%, as caused by the statistical fluctuations for large t. Errors in the least square fit are typically one order of magnitude smaller. Both values for $\sigma_{\alpha\alpha}$ determined either from time integration or from linear fit agree within their errors.

For impurity scattering we use the deterministic dynamics between the randomly distributed scattering events. Scattering times and angles are taken from a random number generator of the NAG Fortran Library based on a multiplicative congruential method. Again correlations are obtained as an average over 10^5 segments from one trajectory covering all of the phase space. For a mostly chaotic phase space correlations behave as in the deterministic dynamics. In the case of substantial oscillating contributions by circle orbits the velocity autocorrelations have to be determined up to a few mean free times τ, e.g., $t \approx 3\tau$. The data in Figs. 7–12 consist of discrete points with $\Delta r_c = 0.025$. All computations were carried through on a hp workstation 715/64.

[1] L.A. Bunimovich and Ya.G. Sinai, Commun. Math. Phys. **78**, 247 (1980); **107**, 357 (E) (1986)

[2] L.A. Bunimovich and Ya.G. Sinai, Commun. Math. Phys. **78**, 479 (1981).

[3] K. Ensslin and R. Schuster, in *III-IV Semiconductor Quantum Systems*, edited by K. Ploog (Institution of Electrical Engineers, New York, in print).

[4] K. Ensslin and P.M. Petroff, Phys. Rev. B **41**, 12 307 (1990).

[5] D. Weiss, *Lateral Superlattices: Magnetoresistance, Hall Effect and Commensurate Orbits* in *Festkörperprobleme*, Advances in Solid State Physics Vol. 31, edited by U. Rössler (Vieweg, Braunschweig, 1991).

[6] Ya.G. Sinai, Russian Math. Sur. **25**, 137 (1970).

[7] P. Garrido and G. Gallavotti, J. Stat. Phys. **76**, 549 (1994).

[8] P.M. Bleher, J. Stat. Phys. **66**, 315 (1992).

[9] A. Zacherl, T. Geisel, J. Nierwetberg, and G. Radons, Phys. Lett. **114**A, 317 (1986)

[10] N.I. Chernov, G.L. Eyink, J.L. Lebowitz, and Ya.G. Sinai, Phys. Rev. Lett. **70**, 2209 (1993); Commun. Math. Phys. **154**, 569 (1993).

[11] E.M. Baskin, G.M. Gusev, Z.D. Kvon, A.G. Pogosov, and M.V. Entin, Pis'ma Zh. Eksp. Teor. Fiz. **55**, 649 (1992) [JETP Lett. **55**, 678 (1992)].

[12] R.S. MacKay, J.D. Meiss, and I.C. Percival, Physica D **13**, 55 (1984).

[13] J.D. Meiss and E. Ott, Physica D **20**, 387 (1986).

[14] T. Geisel, A. Zacherl, and G. Radons, Phys. Rev. Lett. **59**, 2503 (1987); Z. Phys. B **71**, 117 (1988).

[15] R. Fleischmann, T. Geisel, and R. Ketzmerick, Phys. Rev. Lett. **68**, 1367 (1992).

[16] R. Ketzmerick, *Chaos, fraktale Spektren und Quantendynamik in Halbleiter-Mikrostrukturen* (Verlag Harri Deutsch, Frankfurt am Main, 1992).

[17] A. Lorke, J.P. Kotthaus, and K. Ploog, Phys. Rev. B **44**, 3447 (1991).

[18] R. Schuster, K. Ensslin, J.P. Kotthaus, M. Holland, and S.P. Beaumont, Superlattices Microstruct. **12**, 93 (1992).

[19] D. Weiss, M.L. Roukes, A. Menschig, P. Grambow, K. von Klitzing, and G. Weimann, Phys. Rev. Lett. **66**, 2790 (1991).

[20] T.J. Thornton, M.L. Roukes, A. Scherer, and B.P. Van der Gaag, in *Quantum Coherence in Mesoscopic Systems*, edited by B. Kramer (Plenum, New York, 1991).

[21] R. Schuster, G. Ernst, K. Ensslin, M. Entin, M. Holland, G. Böhm, and W. Klein, Phys. Rev. B **50**, 8090 (1994).

[22] A.J. Lichtenberg and M.A. Liebermann, *Regular and Stochastic Motion* (Springer-Verlag, Berlin, 1983).